GPS Solutions, Springer
Accepted for publications, December 2012

LightSquared Effects on Estimated C/N_0, Pseudoranges and Positions

Marco Rao, Cillian O'Driscoll, Daniele Borio, Joaquim Fortuny
European Commission Joint Research Centre, via Enrico Fermi 2749, 21027, Ispra (VA), Italy
Email: (name.surname)@jrc.ec.europa.eu

Abstract

We present experimental results showing the impact of the proposed LightSquared (LS) Long Term Evolution (LTE) signals on both GPS and Galileo civil modulations in the L1/E1 band. The experiments were conducted in radiated mode in a large anechoic chamber. Three Galileo enabled receivers were chosen for the tests and a state of the art GNSS signal generator was used to simulate both GPS and Galileo signals. The LTE signals were generated by an Agilent Programmable Signal Generator (PSG) with a license to generate the signals according to the 3GPP LTE FDD standard. The interference impact was measured in terms of a Carrier-to-Noise power spectral density ratio (C/N_0) ratio degradation, in accordance with the methodology which the LS/GPS Technical Working Group (TWG) established by mandate of the FCC. A model for determining the impact of the LS signal on the considered GNSS signals is provided and is validated against experimental data. It is shown that the Galileo E1 Open Service (OS) signal is marginally more susceptible to this form of interference than the GPS L1 C/A signal due to its greater proximity to the lower edge of the L1 band. The impact of LS interference was further analyzed in terms of pseudorange and position errors. Despite its relevance for most GNSS users, this aspect was not considered by the TWG. Measurement and position domain analysis along with the study of the LS impact on the Galileo OS signals are the major contributions. The analysis confirms the results obtained by the TWG and shows that the receiver front-end plays a major role in protecting GNSS signals against RF interference. While it appears that, for now, the LS network will not be deployed, the approach taken and the results obtained herein can be readily adapted for any future terrestrial mobile network that may take the place of LS.

Keywords: GNSS, interference, LightSquared, TWG

1 Introduction

The proposal of the U.S. company LightSquared (LS) to deploy a network of Long Term Evolution (LTE) base stations operating in a frequency band adjacent to the L1/E1 band caused a debate, lasting more than one year, on the risk that such a system may interfere with existing satellite navigation receivers. The main coexistence issue behind the proposed deployment of LS comes from the high transmit power levels, which are several orders of magnitude greater than those measured at a GNSS antenna. Moreover, the frequency allocation for LS has to be shared with Mobile Satellite Services (MSS), which are presently used to broadcast some GNSS augmentation signals. In fact, the majority of professional multi-frequency multi-constellation GNSS receivers have wide-band front-ends capable of receiving both the GNSS signals at L1/E1 and the MSS augmentation signals. This makes these receivers even more vulnerable to an adjacent band interference located in the MSS band. Consequently, the impact of high power emissions in MSS band can be significant, particularly on professional receivers designed to process wide-band GNSS signals.

However, even if GNSS receivers are equipped with highly selective filters, there will inevitably be some components of the LTE high power signals leaking into the receiver front-end band. In short, no matter whether a GNSS receiver "is looking"' into the MSS band or not, some interfering signal power will pass into the receiver, thereby leading to potential issues in acquiring and tracking GNSS signals. In January 2011 the FCC issued on order granting a conditional waiver to LS to deploy their ground network (FCC 2011). The waiver was conditioned on an in-depth analysis of the impact of the proposed LTE signals on existing GNSS receivers, and the demonstration that the proposed network would not interfere with those receivers. An intensive period of study followed, culminating in the publication of the TWG final report (TWG 2011). This report pointed out a significant degradation of receiver performance across a wide range of receiver types. Subsequently, LS proposed to use only that subset of frequencies within the MSS band which is furthest from the GNSS signals. Such a solution was supposed to significantly reduce interference issues. A second round of tests was then conducted which again showed significant interference effects on GPS devices (NPEF 2012; FAA 2012; Turetzky et al. 2012). It is noted that the tests were conducted on GPS devices not equipped with front-end filters specifically designed to reject interference coming from the MSS bands.

This condition is however common to most commercially avaible receivers. The outcome of these tests resulted in a letter written by the National Telecommunications and Information Administration (NTIA) to the FCC stating that "LightSquared's proposed mobile broadband network will impact GPS services and that there is no practical way to mitigate the potential interference at this time" (NTIA 2012). Note that by "practical way" it is intended that the cost and workload required to modify existing receivers to operate in the presence of LS interference is currently too high to justify the deployment of LS services. Countermeasures enabling the coexistence between GNSS and LS signals exist and can be used to reduce interference problems as demonstrated by Javad (2011). In response to this letter the FCC issued their own statement declaring that they proposed to "vacate the Conditional Waiver Order", thereby revoking LS's authority to deploy their proposed network (FCC 2012).

For the moment, the GNSS community appears to have avoided the deployment of LS, which has been proven to cause significant harmful interference to a large subset of currently deployed receivers. However, as noted in the FCC statement (FCC 2012), spectrum is a precious resource, and the growing desire for wideband mobile internet access will lead to only greater pressure on this resource in the future. The GNSS community is aware of the importance of the spectrum as it faces this problem within the L1 band. While only a few years ago the GPS C/A and P(Y) signals were the only signals broadcast in this band, and they are still the most prevalent, in the future the L1 band will accommodate two new signals from GPS, three from Galileo and possibly more from the Chinese Compass system. To avoid spectral overlap, new modulations were adopted and many of these signals have significant proportions of their power at the edges of the L1 band. This characteristic makes the new signals potentially more susceptible to interference from signals in the MSS band.

Herein, the experimental approach of the TWG is applied to the measurement of the impact of LS signals on both GPS and Galileo civil signals in the L1/E1 band. Three commercial receivers have been chosen as test units, each of which is capable of processing both the GPS C/A code and the Galileo E1b/c signals. We summarize the results presented in Borio et al. (2012) and extend them, discussing not only the receivers' performance in the higher band, but also showing how these receivers perform in the lower band, pointing out the benefits of allocating the LS signal in a band which is further away from the L1 frequencies. Moreover, while in the past only the Carrier-to-Noise power spectral density ratio (C/N_0) degradation was considered, new tests are proposed here on the basis of the measurements obtained from one of the receivers under analysis. The first test is based on the analysis of the pseudoranges produced by a receiver affected by the LS interference and on the comparison with the pseudoranges produced in an interference free scenario. In a second test, the pseudoranges were also used to asses how much the the position estimates are affected in the presence of the LS interference. A least squares solution has been computed to evaluate separately the impact of the interference on positions computed only from GPS or Galileo pseudoranges. The least squares solution allows one to analyze separately the GPS and Galileo position solutions. In addition to this, a least squares solution does not introduce any memory effects as in the Kalman filter used by most commercial receivers to compute the PVT solution. Results relative to the other two receivers are not provided here in order to avoid the repetion of similar findings.

This is the first published set of results showing the impact of the LS signals on Galileo enabled receivers and considering the pseudorange and the position domains. A model of the impact of LS signals on both types of GNSS signal is provided and the model parameters are matched with the experimental results. The technique can be easily extended to other interfering and victim signals, and can therefore be readily used in case any future service is planned for the MSS band. Although all the receivers tested in this work are affected by LS interference, different results may be obtained by considering different devices for example implementing interference mitigation techniques. Filters and dedicated receiver processing (Javad 2011) can enable the coexistence between GNSS and LS signals. The analysis of interference countermeasures is however outside the scope of this work.

Section 2 provides models of both GNSS and LS LTE signals and briefly summarizes the receiver signal processing stages. The experimental setup is described in detail in Section 3 whereas experimental results and model data fitting are provided in Section 4. The paper finishes with the conclusions in Section 5.

2 Signal and System Model

In this section models for the GNSS and LS signals are provided. In this case, GNSS are the victim systems interfered by LS signals. A brief introduction to the operations performed by a GNSS receiver is also provided along with the definition of the metrics that will be used to quantify the impact of LS signals.

2.1 The GNSS signal

The signal at the input of a GNSS receiver in a one-path additive Gaussian channel can be modeled as

$$r(t) = \sum_{l=0}^{N_s-1} y_l(t) + i(t) + \eta(t) \tag{1}$$

which is the sum of N_s useful signals transmitted by N_s different satellites, an interfering term, $i(t)$, and a noise term, $\eta(t)$. Each useful signal, $y_l(t)$ can be made of several elements:

$$y_l(t) = \sum_{h=0}^{N_h-1} e_{l,h}(t) \tag{2}$$

where N_h is the number of transmitted components. An example of composite GNSS is the Galileo E1 interplex (Rebeyrol 2007), which is made of three components: the Open Service (OS) E1b/E1c signals and the Public regulated Service (PRS) E1a component. In the following, only the OS components will be considered.

Each term in (2) can be expressed as

$$e_{l,h}(t) = \sqrt{2C_{l,h}}\, d_{l,h}\left(t-\tau_{0,l}\right) c_{l,h}\left(t-\tau_{0,l}\right) \cos\left(2\pi(f_{RF} + f_{0,l})t + \varphi_{l,h}\right) \tag{3}$$

where $C_{l,h}$ is the power of the h th component of the l th useful signal, $d_{l,h}(\cdot)$ is the navigation message, $c_{l,h}(\cdot)$ is the pseudo-random sequence extracted from a family of quasi-orthogonal codes used for spreading the signal spectrum, $\varphi_{l,h}$ is phase of the h th component of the l th useful signal, $\tau_{0,l}$ and $f_{0,l}$ are the delay and Doppler frequency introduced by the communications channel, and f_{RF} is the centre frequency of the GNSS signal.

The pseudo-random sequence, $c_{l,h}(t)$, is formed by several terms including a primary spreading sequence and a subcarrier:

$$c_{l,h}(t) = \sum_{i=-\infty}^{+\infty} c_{l,h}\left[i \bmod N_c\right] s_{b,h}(t - iT_h) \tag{4}$$

The term $s_{b,h}(t-iT_h)$ is the subcarrier of duration T_h which determines the spectral characteristics of the transmitted GNSS signal. The Galileo E1b/E1c signals adopt Composite Binary Offset Carrier (CBOC) whereas Binary Phase Shift Keying (BPSK) is used for the GPS L1 C/A component. The sequence, $c_{l,h}[i]$, of length N_c defines the primary spreading code of the h th component of the l th GNSS signal.

Due to the quasi-orthogonality of the spreading codes, a GNSS receiver is able to process the N_s useful signals independently. Thus, equation (1) can be simplified as

$$r(t) = y(t) + i(t) + \eta(t) = \sum_{h=0}^{N_h-1} e_h(t) + i(t) + \eta(t) \tag{5}$$

where the index, l has been dropped for ease of notation.

After down-conversion and filtering, the input signal is sampled and quantized. In the following, the impact of quantization and sampling is neglected and, after these operations, equation (5) becomes:

$$r_{BB}[n] = y_{BB}(nT_s) + i_{BB}(nT_s) + \eta_{BB}(nT_s) = y_{BB}[n] + i_{BB}[n] + \eta_{BB}[n] = \sum_{h=0}^{N_h-1} e_{BB,h}[n] + i_{BB}(nT_s) + \eta_{BB}[n] \tag{6}$$

where the notation $x[n]$ is used to denote a discrete time sequence sampled at the frequency $f_s = \dfrac{1}{T_s}$. The subscript "BB" is used to denote a filtered signal down-converted to baseband. In equation (6) ,

$$e_{BB,h}[n] = \sqrt{C_h}\, d_h\left(nT_s - \tau_0\right) c_h\left(nT_s - \tau_0\right) \exp\left\{ j2\pi f_0 nT_s + j\varphi_h \right\} \tag{7}$$

it is noted that the different components of $y_{BB}[n]$ are also characterized by quasi-orthogonal codes and subcarriers. Thus, a GNSS receiver can, in general, process the different components of $y_{BB}[n]$ independently. Under this hypothesis, equation (6) can be further simplified as

$$r_{BB}[n] = \sqrt{C}\, d\left(nT_s - \tau_0\right) c\left(nT_s - \tau_0\right) \exp\left\{ j2\pi f_0 nT_s + j\varphi \right\} + \eta_{BB}[n] \tag{8}$$

where the index h has been removed for ease of notation.The model assumed for $i_{BB}[n]$ is briefly discussed in Section 2.2 along with a brief description of the LS signal characteristics. The noise term, $\eta_{BB}[n]$, is assumed to be an additive white Gaussian noise with variance σ^2_{BB}. σ^2_{BB} depends on the filtering, down-conversion and sampling strategy applied by the receiver front-end and can be expressed as $\sigma^2_{BB} = N_0 B_{RX}$ where B_{RX} is the front-end bandwidth and N_0 is the Power Spectral Density (PSD) of the input noise $\eta(t)$. The ratio between the carrier power, C, and the noise PSD, N_0, defines the C/N_0, one of the main signal quality indicators used in GNSS.

2.2 The LS signal

The LS signals that could potentially affect GNSS operations will be broadcast in the bands (TWG 2011)

$$\begin{cases} 1526.0\text{–}1536.0 \text{ MHz} - \text{Lower Band} \\ 1545.2\text{–}1555.2 \text{ MHz} - \text{Upper Band} \end{cases} \tag{11}$$

These signals will be used for the LS down-link. Signals used for the paired up-link could have an impact on GLONASS receivers but are not considered in this study.

Each band can be configured for either a 5 or 10 MHz transmission, for a total of four possible configurations:

Lower band, 5 MHz: 1531.0–1536.0 MHz
Lower band, 10 MHz: 1526.0–1536.0 MHz
Upper band, 5 MHz: 1550.2–1555.2 MHz
Upper band, 10 MHz: 1545.2–1555.2 MHz

The down-link signals are OFDM modulated and can occupy up to two 10 MHz bands. The orthogonality of the different carriers allows for an efficient use of the spectrum. Fortuny-Guasch et al. (2011) considered the Digital Video Broadcast – Terrestrial (DVB-T) signal as a potential interference source for GPS. DVB-T is also OFDM modulated and the authors showed that an OFDM signal, in the time domain, can be effectively modeled as a zero mean Gaussian random noise process whose spectral characteristics depends on the allocated carriers. If all the carriers were used then its spectrum would be flat.

In this paper, the results obtained by Fortuny-Guasch et al. (2011) are applied to the LS signal, which is modeled as a zero mean Gaussian random noise process. The spectral characteristics of $i_{BB}[n]$ depend however on the LS transmission filter and the GNSS receiver front-end. The characteristics of the LS transmission filter and the attenuation provided by the GNSS antenna used for the experiments are briefly discussed in Section 3.

2.3 The correlation process

In standard GNSS receivers, the sequence $r_{BB}[n]$ is correlated with local replicas of the useful signal code and carrier as shown in Fig. 1 .

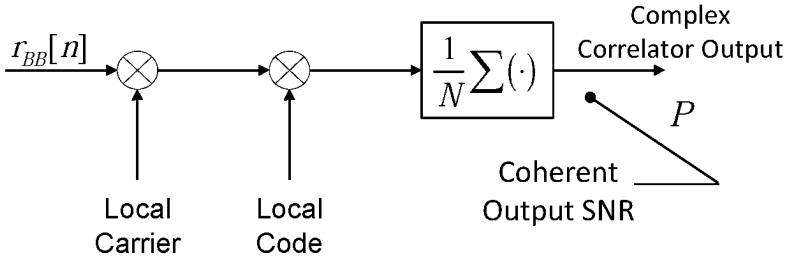

Figure 1 - Schematic representation of the correlation process performed by a GNSS receiver. The coherent

output SNR is evaluated at the correlator output.

The complex correlator output is computed as

$$P = \frac{1}{N}\sum_{n=0}^{N-1} r_{BB}[n]c\left(nT_s - \tau\right)\exp\left\{-j2\pi f_d nT_s - j\varphi\right\} \tag{12}$$

where τ, f_d and φ are the code delay, the Doppler frequency and the phase tested by the receiver. N is the number of samples used for computing a correlator output and $T_c = NT_s$ is the coherent integration time. It is noted that the computation of correlator outputs is essential for the proper functioning of a GNSS receiver and they are used both in acquisition and tracking (Kaplan 2005), the main receiver operating modes. Thus, the quality of a GNSS signal can be defined after correlation as (Betz 2001, 2002):

$$SNR_{out} = \max_{\tau, f_d, \varphi} \frac{|E\{P\}|^2}{\frac{1}{2}Var\{P\}} \tag{13}$$

where SNR_{out} is the coherent output SNR. The factor 1/2 in equation (13) accounts for the fact that P is a complex quantity and only the variance of its real part is considered. The loss experienced at the correlator output due to the presence of LS interference can be determined as the ratio between the measured SNR and the ideal coherent output SNR determined in the absence of interference.

It is noted that equation (12) is a linear operation and the impact of signal, noise and interference on the correlator outputs can be evaluated separately. The signal component is considered as a deterministic term that does not contribute to the correlator variance. Both $i_{BB}[n]$ and $\eta_{BB}[n]$ are modeled as zero mean random processes that only contribute to the variance of the correlator outputs. Using the results derived in (Betz 2001, 2002; Borio 2008), it is possible to express the coherent output SNR as

$$SNR = \frac{C}{\frac{N_0}{2T_c} + \frac{C_i}{2T_c}k_a} = 2\frac{C}{N_0}T_c\frac{1}{1+\frac{C_i}{N_0}k_a} \tag{14}$$

where C_i is the interference power and k_a is the Spectral Separation Coefficient (SSC) defined as (Betz 2001, 2002)

$$k_a = \int_{-B_{RX}/2}^{B_{RX}/2} G_i(f)G_c(f)df \tag{15}$$

where $G_i(f)$ is the normalized PSD of the LS signal after front-end filtering. It is noted the adoption of sharp front-end filters can significantly reduced the amount of interference power entering a GNSS receiver as demonstrated by Javad (2011). The PSD $G_i(f)$ is normalized such that

$$\int_{-B_{RX}/2}^{B_{RX}/2} G_i(f)df = 1 \tag{16}$$

The term $G_c(f)$ models the effect of the correlation on the interfering signal. Correlation can be modeled as an additional filtering stage and $G_c(f)$ can be shown to be well approximated by the PSD of the subcarrier used in the de-spreading process. $G_c(f)$ is also normalized to have a unit integral. It is noted that different subcarriers lead to different $G_c(f)$ and thus, $i_{BB}[n]$ will have different effects depending on the type of modulation considered.

The ideal coherent SNR is obtained by setting $k_a = 0$:

$$SNR_{ideal} = 2\frac{C}{N_0}T_c \tag{17}$$

and the loss due to the interference presence is given by

$$L_i = \frac{1}{1+\frac{C_i}{N_0}k_a} \tag{18}$$

In the following, the loss L_i will be empirically determined. Most GNSS receivers estimate the C/N_0 by first estimating the coherent output SNR (Parkinson 1996). The C/N_0 is then obtained using the relationship in (17). For this reason, C/N_0 estimates are simply a scaled version of the coherent output SNR and are impacted by the presence of an interfering signal. Thus, they can be used for determining L_i and, hence, empirical estimates of k_a.

The PSDs of all signals considered in this paper are shown in Fig. 2. Note that the GNSS PSDs are normalised to unit power over an infinite bandwidth. In reality the signal will be bandlimited, and hence the PSD will be larger in-band. Secondly, an ideal brick wall filter has been assumed for the LS LTE signals, whereas in reality there will be some signal leakage out of band. Note also that, while the transmitted GNSS signals are nominally bandlimited to a 30 MHz bandwidth for GPS and approximately 40 MHz for Galileo, what matters in terms of the impact of the LTE on GNSS signal processing is the locally generated replica, which may be generated with even larger bandwidths.

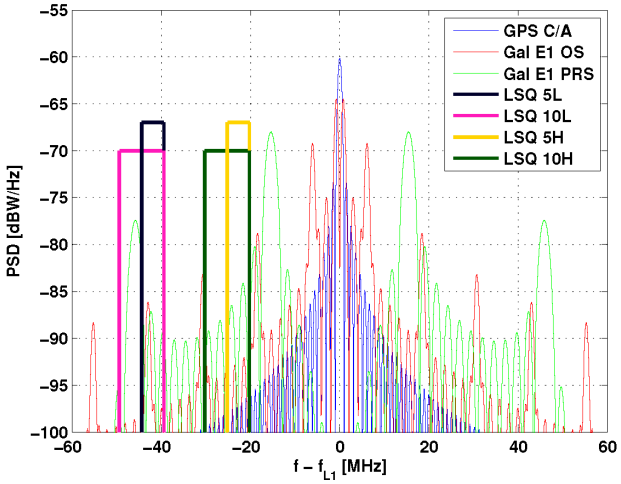

Figure 2 - PSDs of all signals considered. The L1 frequency is at the origin

3 Experimental Setup

A set of commercial GPS/Galileo receivers were tested in a radiated mode in a large anechoic chamber. The primary purpose of these tests was to evaluate the difference between the impact of LS LTE signals on GPS and Galileo. These experiments were performed in accordance with the procedures described in the precision and timing receivers section of the TWG final report (TWG 2011). The obtained results are limited to a smaller number of receivers, as the emphasis in this case is on the comparison of the impact on GPS and Galileo. Therefore, only receivers capable of processing both GPS L1 and Galileo E1 signals have been tested.

The radiated tests described herein were performed in a large anechoic chamber. A schematic diagram of the experimental setup is given in Fig. 3 and a panoramic view of the chamber is shown in Fig. 4 .

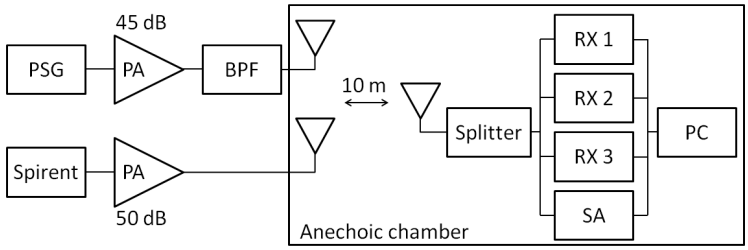

Figure 3 - Schematic overview of the experimental setup for the radiated tests.

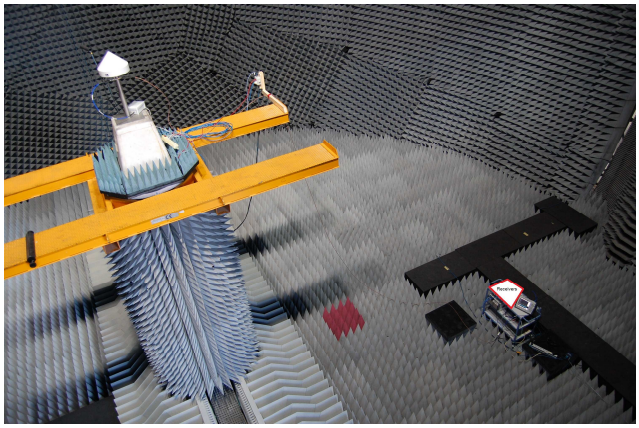

Figure 4 - View of the anechoic chamber: receiving antenna and receivers.

GNSS signals were generated by a Spirent GSS8800 simulator, whereas the LS LTE component was provided by an Agilent E8267D Programmable Signal Generator (PSG), with a license for the 3GPP LTE specifications (revision 9), cascaded with a 10 W RF amplifier.

The parameters were configured as described in the TWG final report. Two separate RF filters were obtained to limit the LS signals band. These were the RF Morecomm RMC1531B10M01 and RMC1550B10M01 Bandpass Filters (BPF), for the lower and upper frequency bands respectively. These, again, are the same filters as were used by the TWG.

The BPF frequency response was measured by a calibrated network analyzer and the result is shown in Fig. 5. Note from the figure that the filters themselves have non-zero gain within the L1/E1 band. This results in a small fraction of the LTE signal power leaking into the GNSS band. While the fraction is small, if the LTE signal power is sufficiently large, this can result in a significant amount of power in the GNSS band.

The GNSS and LTE signals were broadcast from adjacent antennas mounted on a sled, which was positioned at zenith within the chamber. The LTE signals were broadcast from a linearly polarized horn antenna while the GNSS signals were broadcast from an RHCP radiating antenna. A single receive antenna, a survey grade antenna with a choke-ring and radome, was placed on a test platform directly under the transmit antennas at a distance of approximately 10 m. Thus, both the GNSS and LTE signals are received at zenith. Note that this is not a realistic scenario, but is again in keeping with the TWG procedure. The frequency response of this antenna to a linearly polarised test signal was measured and the results are given in Fig. 6. Note that this is an active antenna and hence has a peak gain that is approximately 6 dB greater than the gain in the upper LTE band.

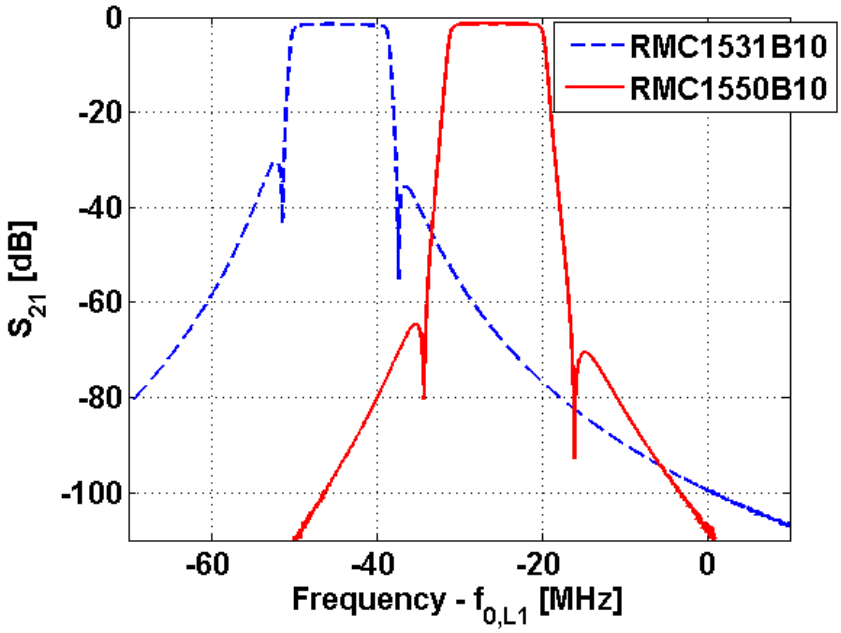

Figure 5 - Frequency response of the RF Morecomm RMC1531B10M01 and RMC1550B10M01 BPF, measured by a network analyzer.

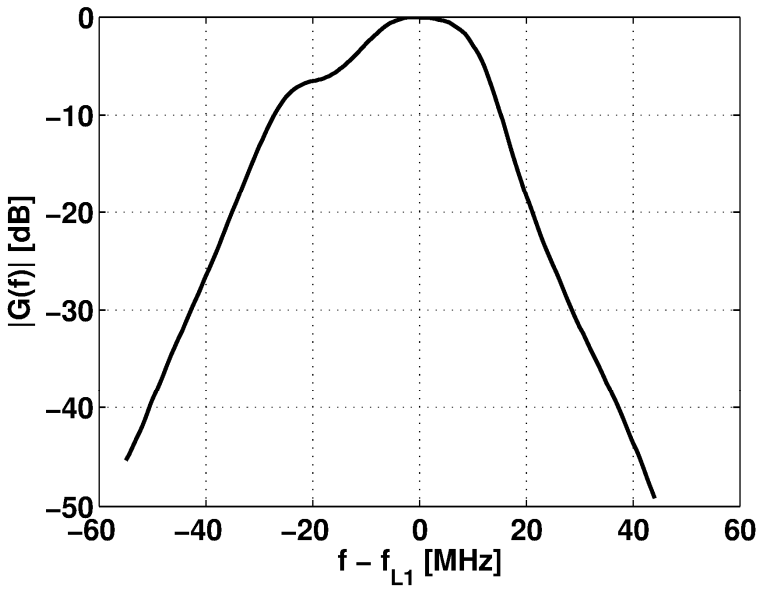

Figure 6 - Frequency response of the GNSS antenna connected to the receivers, with respect to the L1 band centre frequency.

The impact of the GNSS antenna on the PSD of the signals entering the receiver is shown in Fig. 7. Note that the lower LTE frequency band is attenuated by nearly 20 dB with respect to the upper band. For different antennas with different characteristics the precise impact on the LTE signals can vary dramatically. In addition, this plot does not account for further filtering stages within the receivers, which may also have a significant impact on the signals as processed by the receiver (Javad 2011).

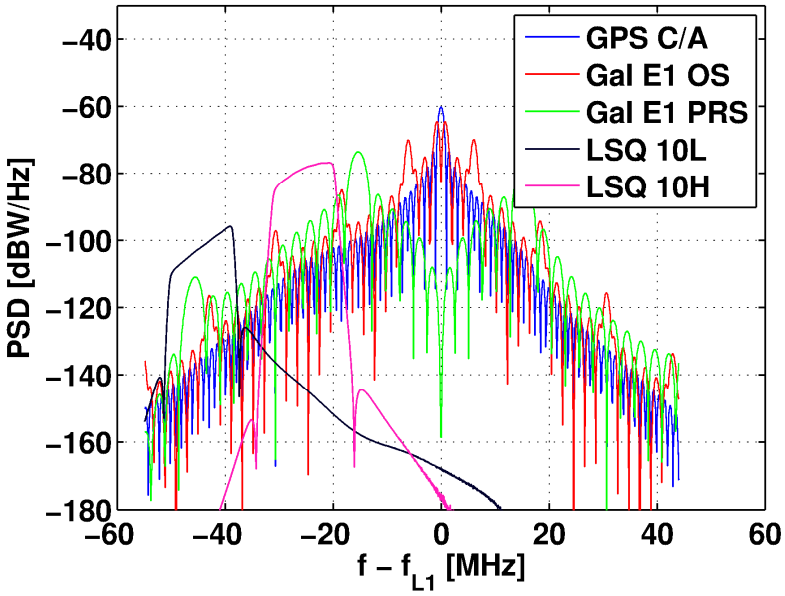

Figure 7 - PSD of the GNSS and LTE signals after signal conditioning in the antenna.

The GNSS antenna was connected via a four way splitter to the three receivers under test and to a spectrum analyzer for calibration. The three considered receiver models are not disclosed here nor in the following.

In the following sections, the "LTE Power" used in the figures and equations related to the radiated tests corresponds to the power measured at the output of a polarization matched, calibrated antenna with 0 dB gain towards the LTE transmitter. The power is measured using a calibrated spectrum analyser as the total power in the 5 or 10 MHz bandwidth of the LTE signal. As such it does not account for power under the skirt of the BPF.

4 Results

This section shows the results of the measurement campaign. It is divided in five subsections. In the first, the impact of the LS on GNSS signals is assessed by measuring the loss of C/N_0 with respect to an interference-free baseline. In the second, the experimental data is fitted to the model of (18). In the third subsection, remarks on GPS and Galileo performance in the presence of LS signal are made. The last two sections focus on the pseudorange measurements obtained from only one of the receivers: the fourth section is focused on the comparison of the pseudoranges computed in the interference free and in the interfered scenarios, while the fifth and final subsection gives a comparison between the position errors performed when those pseudoranges are processed by means of a least squares algorithm.

4.1 Experimental Results on Galileo E1c and GPS L1 C/A

The test procedure was conducted as follows. First a baseline test was conducted, wherein the equipment was configured, but the PSG was turned off. In this case no LTE signals were broadcast in the chamber. A static receiver scenario was simulated by the Spirent simulator, with 8 GPS and 8 Galileo satellites in view. The scenario continued for a period of just under two and a half hours during which time measurements were recorded from the receivers under test at a 1 Hz rate. All receivers recorded C/N_0 measurements in addition to position solutions and raw pseudorange and Doppler measurements. The C/N_0 measurement results are presented in the following, while considerations on the pseudoranges and position estimates are reported in the second part of the section.

Once the baseline test was completed, the following procedure was repeated for each of the LTE configurations. The Spirent simulator was configured with the same static scenario as in the baseline test, while the PSG was configured to transmit a power of P_{Tx} = -90 dBm, which corresponds to a received power of ≈ -104.5 dBm. This level was maintained for the first 5 minutes of the test. The value of P_{TX} was then increased by 1 dB every 1 minute, with the power level held constant during each 1 minute interval, up to a maximum value of P_{Tx} = -20 dBm. This power level was maintained for two minutes, then the procedure was reversed, with the power level decreasing

by 1 dB every 1 minute down to the minimum level.

The performance metric chosen for analysis in this paper is the C/N_0 loss L_i defined in (18), which can be estimated from

$$L_i = \left(C / N_0\right)_{\text{test}} - \left(C / N_0\right)_{\text{baseline}} \tag{19}$$

Where $(C/N_0)_{\text{test}}$ is the C/N_0 measured during the testing phase and $(C/N_0)_{\text{baseline}}$ is that measured during the baseline test. A loss value is computed for each satellite in view and the result is averaged over all signals of the same type (GPS or Galileo).

In order to fit the experimental data to the simple model of (18), it is necessary to group the C/N_0 loss according to the received LTE power. The results are shown in Fig. 8. While it is clear from the figure that the signal structure has some impact on the C/N_0 loss, it is also evident that the variation between receivers is substantially greater than the variation between signals. While a more detailed analysis is given in the following section, it is clear from Fig. 8 that, for the upper frequency bands 5H and 10H, there can be significant impact on both GPS and Galileo signals for received LTE signal powers as low as -80 dBm.

The same procedure was applied for the lower LTE frequency bands, where in this case the LTE signal power ranged from -75 to -5 dBm in 1 dBm increments. This resulted in received power levels in the range of approximately -90 to -20 dBm. By observing Fig. 9, it is interesting to note that, as would be expected, the impact of the lower frequency band is much reduced for the same received LTE signal power as in the upper frequency bands. In fact, for the range of received signal power considered here, the loss in C/N_0 in receiver 1 is negligible. However, for the other two receivers, at a received power level of -20 dBm the average C/N_0 loss is at least 10 dB for both frequency bands and for both GPS and Galileo signals.

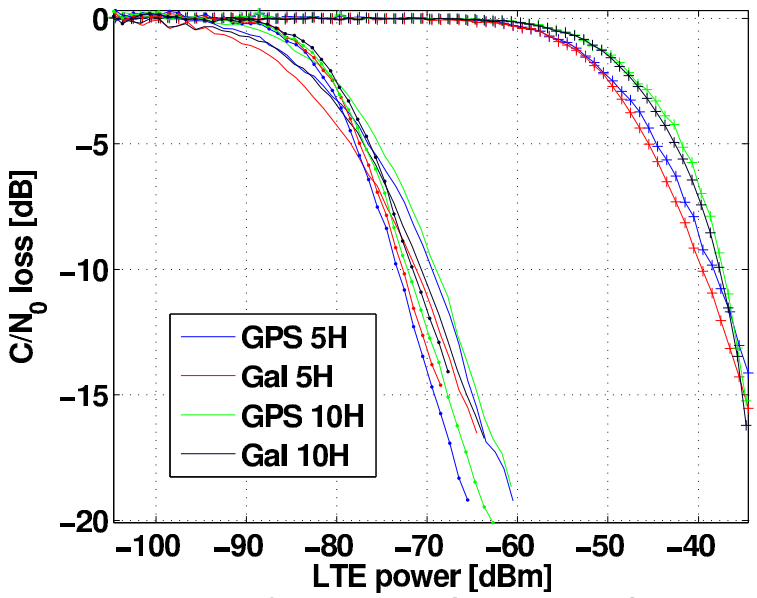

Figure 8 - Mean C/N_0 degradation: upper frequency band. `+': Receiver 1; `-': Receiver 2; ` ': Receiver 3

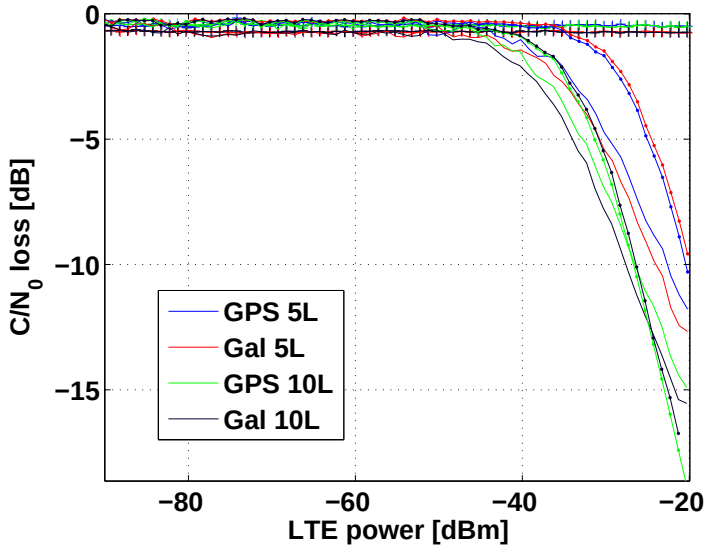

Figure 9 - Mean C/N_0 degradation: lower frequency band. `+': Receiver 1; `-': Receiver 2; ``': Receiver 3

It is interesting to compare the results of Figs. 8 and 9 with those obtained by the TWG. Fig. 9 above can be directly compared with Figs. 36 and 37 of the TWG report (TWG 2011), which were reproduced as Fig. 13 in Boulton et al (2011). While it is not possible to identify the receivers used in this test with specific receivers used in the TWG tests, it is clear that the results obtained herein fall within the bounds of those obtained by the TWG. For example, Figs. 36 and 37 of the TWG report show the knee in the curve occurs in the region of -60 to -15 dBm received power, with a significant group of receivers exhibiting the knee at about -35 dBm, similar to receivers 2 and 3 in Fig. 9 above. This result is similar to that presented in Table 5 of the NPEF report (NPEF 2012).

For the upper frequency band results it is necessary to consult Fig. 97 in Appendix H of the TWG report. This figure shows the received LTE power at which a 1 dB drop in C/N_0 was observed for each receiver under test. In the TWG report 50 % of all receivers tested experienced at least a 1 dB drop at a received LTE power of -56 dBm, while the 10 % point was at -81 dBm. Our small sample also falls within these bounds, although we might expect the percentiles to be a little lower given our data since receivers 2 and 3 experience the 1 dB point at about -80 dBm.

The novel contribution of the above results, therefore, is to demonstrate that the impact of LS signals on the Galileo E1 OS signals is only marginally different to that on the GPS L1 C/A signal.

4.2 Model Fitting

In order to validate model (18), some simplifying approximations have been made. Firstly, it is assumed that the noise PSD is given by N_0 = -204 dBW/Hz. Secondly, since no accounting has been made for the impact of quantization losses in the model, only data for which the C/N_0 loss is less than 5 dB is considered for the fit. As the interfering power increases to a level commensurate with the total noise power in the receiver front-end, then the receiver AGC will respond by reducing the gain, thereby increasing quantization losses for the useful signals. The model of (18) does not include the impact of these quantization losses and so can be viewed as a lower bound on the loss.

To fit the model to the data a simple least-squares approach was taken. Measurements were formed by taking the C/N_0 loss in linear units (denoted L_i) and computing:

$$z = \frac{1}{L_i} - 1 \tag{20}$$

Comparing this with equation (18), then the model predicts the following relationship:

$$z = \alpha C_i \tag{21}$$

Where $\alpha = k_a/N_0$. Thus, given a vector of measurments $\mathbf{z}$ and the corresponding vector of intefering signal power $\mathbf{C}_i$, then the least-squares estimate of the parameter α is given by:

$$\hat{\alpha} = \left(\mathbf{C}_i^T \mathbf{C}_i\right)^{-1} \mathbf{C}_i^T \mathbf{z} \tag{22}$$

The SSC is then estimated as follows:

$$\hat{k}_a = N_0 \hat{\alpha} \tag{23}$$

The best fit parameters obtained are recorded in Table 1. The first thing to note is that the receivers can quickly be divided into two groups. Receiver 1 has signficantly lower SSCs than the other two receivers by approximately 30 dB. This is a significant difference, as was also seen in the previous figure. The most likely explanation for this is due to the differences in front-end filtering between the three receivers. It is most likely that the front-end of receiver 1 is effectively filtering out the major (out of band) component of the LTE signal, while those of receivers 2 and 3 are allowing much of this signal through. The results obtained from receiver 1 shows that the coexistence between LS and GNSS may be possible if careful front-end filtering is implemented. Indeed, the FCC is proposing the development of a set of receiver standards that any GNSS receiver must meet in order to claim protection from interference from adjacent bands under FCC rules. On the other hand, any newly introduced rules in this regard will not help to protect receivers already deployed in the field, many of which would require some form of modification to provide extra protection from LS signals.

Secondly, for most of the configurations the results for the upper 5 MHz are slightly worse (by up to 3 dB) than those for the upper 10 MHz. This is perhaps to be expected, since the spectral density of the 5 MHz signal will be twice as large as that for the 10 MHz signal for the same total signal power. Note that this would appear to confirm the hypothesis that receiver 1 has a narrower front-end filter, since the difference in SSC between the 5 and 10 MHz LTE signals is approximately 3 dB in this case.

Table 1: Estimated SSC Values [dB Hz^{-1}]

LTE Frequency band					
Rx	GNSS	5L	10L	5H	10H
1	GPS	-	-	-125.98	-128.77
	Galileo	-	-	-125.12	-128.01
2	GPS	-171.68	-168.51	-93.74	-95.19
	Galileo	-170.63	-167.70	-93.76	-93.26
3	GPS	-176.78	-170.26	-93.55	-94.35
	Galileo	-177.01	-170.88	-93.86	-94.74

4.3 Comparison of GPS and Galileo Signals

Due to the fact that the Galileo E1 OS signal has a larger bandwidth, with more signal energy near to the LS LTE signal than the GPS L1 C/A signal, it would be expected *a priori* that it would be more susceptible to this type of interference. In other words, the SSC for the Galileo E1 OS signal should be greater than that for the GPS C/A signal. In fact, from Table 1 we can see that this is generally the case, except for the case of receiver number 3.

It is difficult to determine a cause for this unexpected behaviour for this receiver, as we do not know what type of processing is being performed within. In fact, even though the SSC for the Galileo signal is generally greater than that for L1 C/A, the difference is slight, being less than 1 dB in all cases. By far the greatest contribution to the difference in performance between the various receiver types arises due to differences in front-end filtering. The difference in loss between the receivers is significant, confirming that the receiver hardware, rather than the signal structure, is the deciding factor in this case. It is also clear that there is little difference due to the choice of the 5 or 10 MHz LTE band.

4.4 Effects of the interference on the estimated pseudoranges

The results presented in this section are obtained following the same procedure adopted in the preceeding C/N_0 ratio tests. The baseline is again used as a reference to assess the performance of the receiver in the presence of the LS interference.

Only one of the three receivers will be considered for the pseudorange and positioning tests, since no relevant differences arise among the three receivers. The pseudorange measurements are obtained directly from the receiver. The parameter chosen to evaluate the receiver performance is the variance of the pseudoranges. It is noted that pseudoranges are time-varying and the sample variance cannot be used directly to determine the quality of the measurements. The time-varying mean of the pseudorage has to be at first estimated and removed from the measurements. For this reason, the following procedure has been adopted. For the *i*-th satellite, an estimate of the

pseudorange mean, $\tilde{\rho}_i[k]$, is obtained as a 5th order polynomial fit to the pseudorage measurements, $\rho_i[k]$. The fit is performed over an analysis window of 100 samples. The difference

$$\Delta\rho_i[k] = \rho_i[k] - \tilde{\rho}_i[k] \tag{24}$$

is then used for the variance computation. Since $\Delta\rho_i[k]$ is zero mean the variance is estimated as

$$\sigma_i^2[j] = \frac{1}{M_s - 1} \sum_{k=jM_s}^{(j+1)M_s-1} \Delta\rho_i^2[k] \tag{25}$$

where $M_s = 60$ is the number of samples used for the variance estimation. Note that $\sigma_i^2[j]$ is computed over different epochs, considering non-overlapping blocks of measurements. This approach is adopted to capture the pseudorange variance for different interference power levels. The LS power is constant over each block of measurements and j is used to indicate the different processing epochs. Variance (25) is computed in the presence of LS interference. The same approach is adopted to compute $\sigma_{i,BL}^2[j]$, the variance of the pseudoranges in the absence of interference. Finally, the mean variance increase, $\Delta\sigma^2[j]$, is computed as

$$\Delta\sigma^2[j] = \frac{1}{N_s} \sum_{i=1}^{N_s} \left(\sigma_i^2[j] - \sigma_{i,BL}^2[j] \right) \tag{26}$$

The term $\Delta\sigma^2[j]$ is the variance increase for the *j*th processing epoch avaraged with respect to all satellites in view. This metric has been selected in order to isolate the contribution of the interference alone. Noise and interference are modeled as additive independent processes and the variance of the measurements in the presence of interference is given by sum of the noise and interference variances. Equation (26) allows one to isolate the interference variance. In the following figures, the square root of the parameter in (26) is plotted.

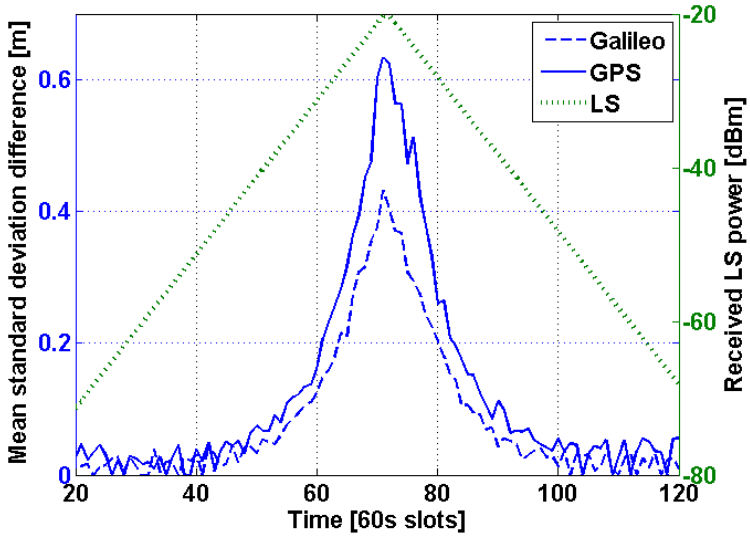

Figure 10 – Standard deviation increase of the pseudorange measurements as a function of time and LS power. LS interference in the lower 10MHz band

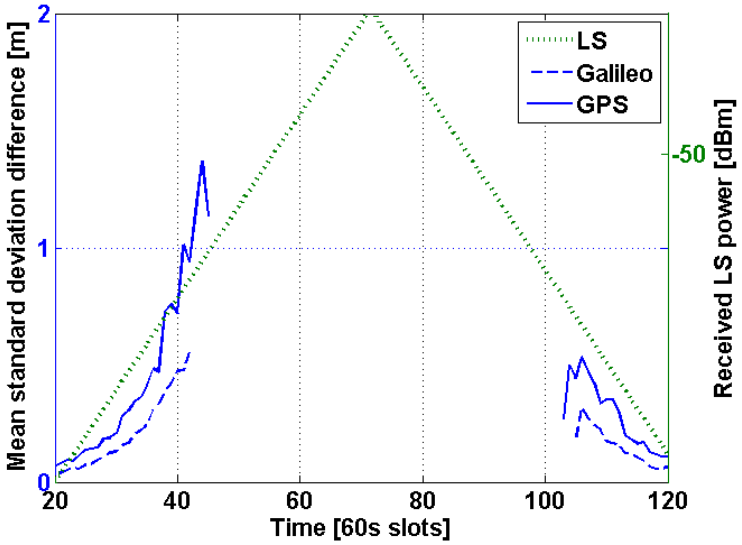

Figure 11 - Standard deviation increase of the pseudorange measurements as a function of time and LS power. LS interference in the upper 10MHz band

As can easily be noted, the case shown in Fig. 11 where the considered LS signal is broadcast in the upper band is the most disruptive. In this case, no pseudorange measurements are available in the central part of the test. When the LS signal is instead broadcast in the lower band as in Fig. 10, pseudoranges are available for the whole duration of the test, although they are noisier than in the interference free scenario.

4.5 Effects of the interference on the estimated position

The effects of LS interference has previously been analyzed in terms of C/N_0 degradation. Although this is a meaningful indicator of the signal quality, it is difficult to assess the receiver positioning performance from this parameter. Nonetheless, the estimated position is the most important measurements provided by a receiver and for this reason the postioning error due to the presence of the LS signal will be discussed in the following.

A simple tool to process the ephemeris and the pseudoranges logged by the receiver under test has been developed. This tool was necessary for two reasons. First, it provides the position solution on the basis of the GPS and Galileo measurements separately, whereas the positioning algorithm adopted by the receiver under test is not known and it implements a joint GPS and Galileo solution. Moreover, the considered position solution is obtained by means of a simple least squares adjustment, which is memory-less. On the contrary, the receiver under test implements a navigation filter, so that each position solution dependents on the previous fixes and the filtering adopted by the receiver.

The scenario is the same used in the previous experiments, where the antenna is kept static and 16 satellites (8 GPS and 8 Galileo) are in view. The first two plots in Fig. 12 show the standard deviation of the position estimate error when the LS interference is absent.

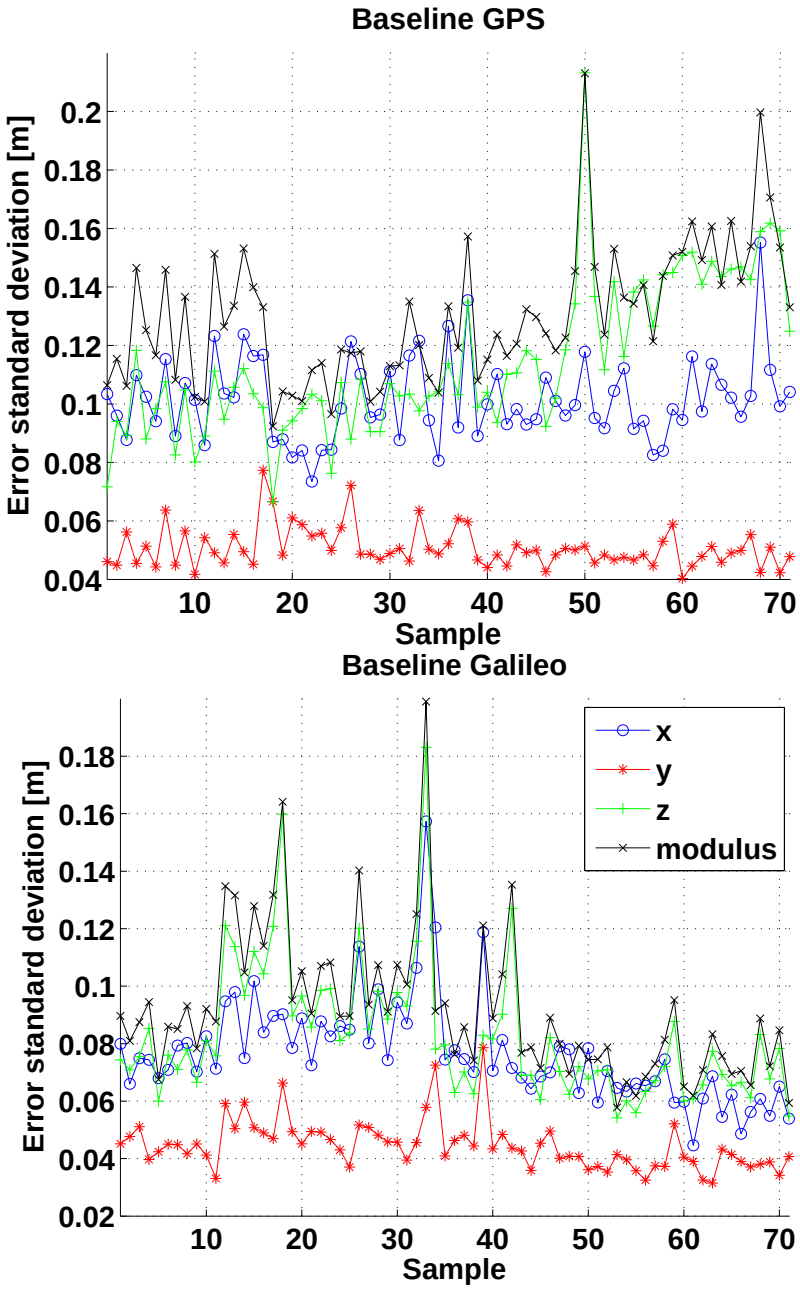

Figure 12 – Receiver performance in the absence of the LS interference. GPS only (top) and Galileo only (bottom) solutions

The standard deviations are computed in the 60 seconds windows which are affected by a constant interference power in the following experiments. Once the baseline performance have been assessed, the positioning errors when the LS signal is broadcast can be determined. The considered performance index is the same adopted for the pseudoranges. In this case, the variance is computed with respect to the true position set in the Spirent simulator.

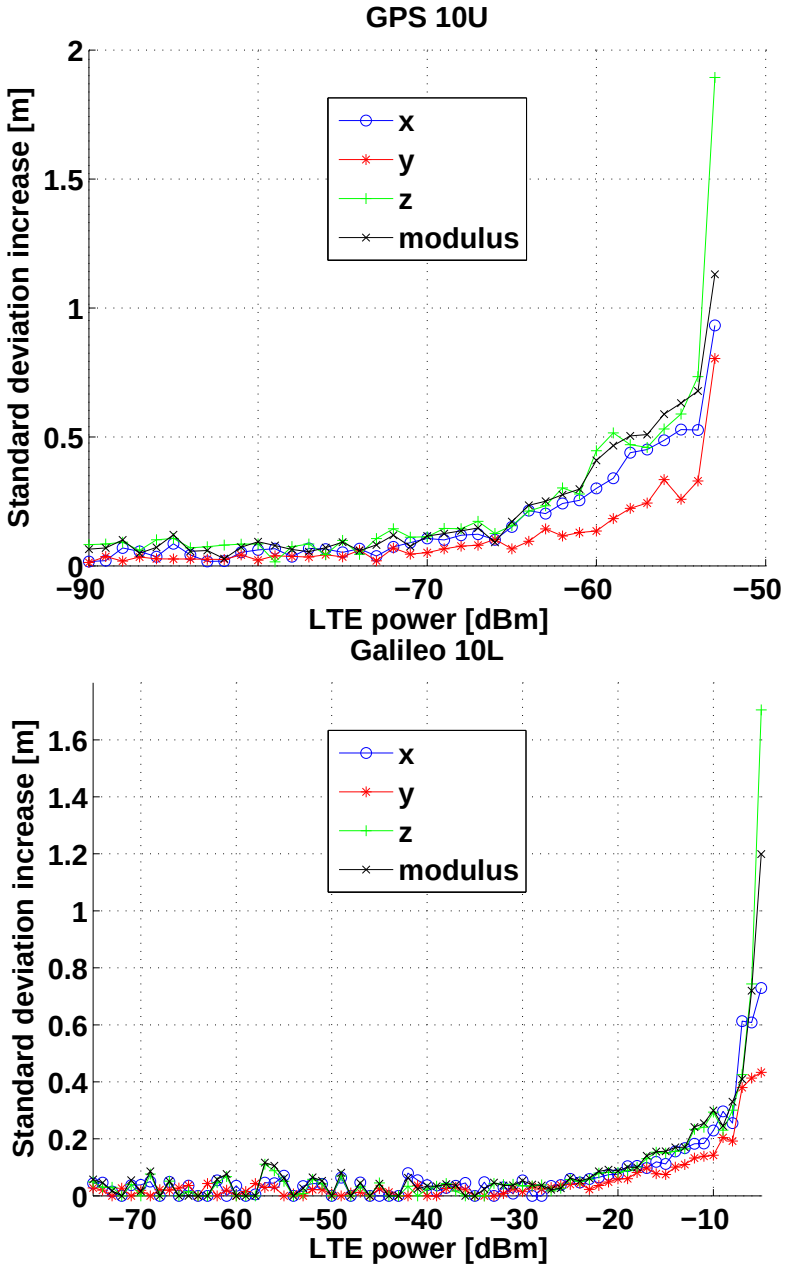

Figure 13 - Standard deviation increase of the position error in the presence of the LS interference in the upper (top) and lower (bottom) 10 MHz band with respect to the interference free scenario - GPS only

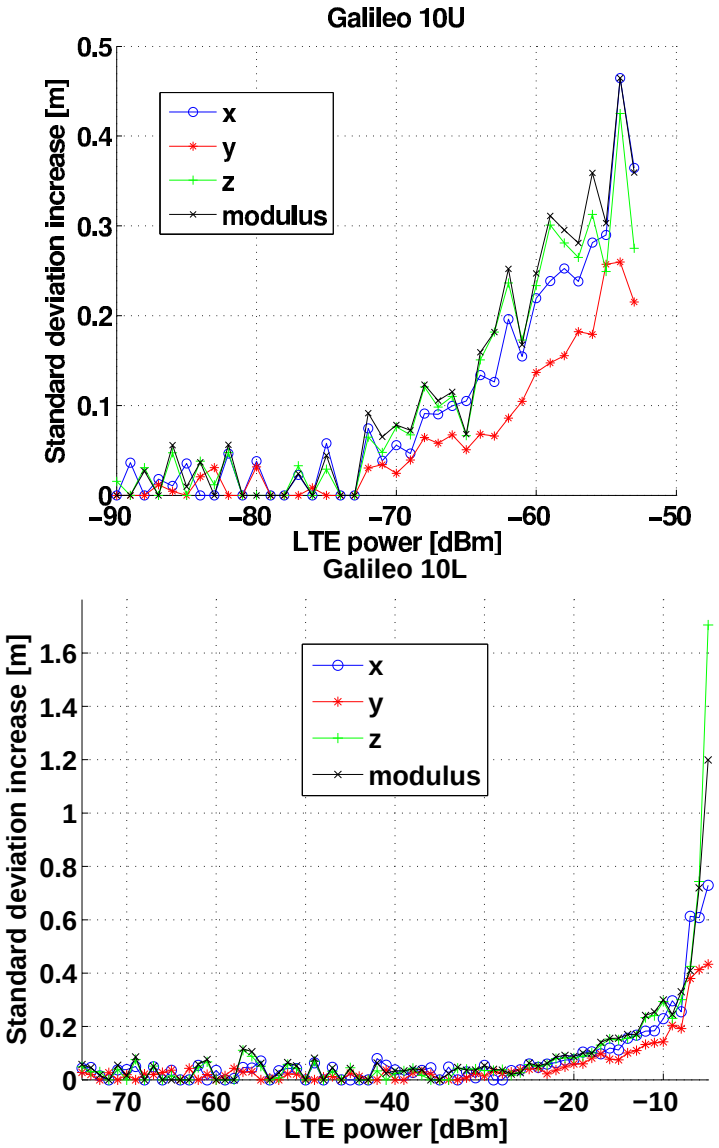

Figure 14 – Standard deviation increase of the position error in the presence of the LS interference in the upper (top) and lower (bottom)10 MHz band with respect to the interference free scenario – Galileo only

The results shown in Figures 13 and 14 are in accordance with the one obtained for the pseudoranges. As expected, noisier pseudoranges lead to less accurate position estimates. The figures provided above allow one to better understand how LS interference affects position estimates. While the upper band case is extremely disruptive and worsen quickly the positioning performance of a receiver, the lower band case appears to be less harmful, since this signal can be disruptive only in proximity of a LS basestation, where significant power can enter a GNSS receiver.

5 Conclusion

We presented experimental results on the effects of the proposed LS LTE terrestrial mobile network on GPS C/A and Galileo civil signals in the L1/E1 band. The impact of the LS signals has been measured in terms of C/N_0 loss according to the methodology adopted in the TWG report (2011). Three high-end Galileo/GPS receivers where used for the analysis. The C/N_0 loss has been characterized using a simple model able to effectively interpolate the esperimental results. Moreover, the impact of the LS signals has also been assessed with respect to the measured pseudoranges and estimated positions: two aspects which were not considered in the past.

In accordance with the results obtained by the TWG, it has been found that there is a significant difference in the level of impact suffered by different receivers. The signal type (GPS C/A or Galileo E1 OS) also affects the degree to which the interference degrades the receiver performance, albeit to a much lower extent. While it would be predicted that the Galileo OS signal would experience greater degradation than the GPS C/A signal, this was found to be the case only for two out of the three receivers tested. Note that the receivers under test did not implement any countermeasure against LS interference. Narrow filters and special processing techniques may make the coexistence between GNSS and LS possible.

The results are in accordance with the ones shown in the TWG final report (2011) and extends the set of tested signals. The methodology adopted in this study is general and can be adopted for the analysis of any available GNSS signal as demostrated here for the Galileo E1b/c signals.

References

Betz JW (2000) Effect of narrowband interference on GPS code tracking accuracy. Proc. ION NTM, pages 16-27, Anaheim, CA

Betz JW (2001) Effect of Partial-Band Interference on Receiver Estimation of C/N_0. Proc. ION NTM, pages 817 - 828, Long Beach, CA

Borio D (2008) A statistical theory for GNSS signal acquisition. PhD Thesis, Politecnico di Torino

Borio D, O´Driscoll C, Rao M, Cano E, Fortuny J (2012) Compatibility Analysis Between LightSquared Signals and L1/E1 GNSS Reception. Proc. IEEE/ION PLANS, Myrtle Beach, SC, April 24-26

Boulton P, Borsato R, Butler B, Judge K (2011) GPS Interference Testing: Lab, Live, and LightSquared, Inside GNSS, pages 32-45, May/June.

FAA (2012) Status Report: Assessment Of Compatibility Of Planned Lightsquared Ancillary Terrestrial Component Transmissions In The 1526-1536 MHz Band With Certified Aviation GPS Receivers. Tech. rep., Federal Aviation Administration, http://www.ntia.doc.gov/files/ntia/publications/. Accessed 14 September 2012

FCC (2011), Order and Authorization in the Matter of LightSquared Subsidiary LLC Request for Modification of its Authority for an Ancillary Terrestrial Component. http://www.fcc.gov/document/lightsquared-subsidiary-llc-0. Accessed 14 September 2012

FCC (2012) , Statement From FCC Spokesperson Tammy Sun On Letter From NTIA Addressing Harmful Interference Testing Conclusions Pertaining To LightSquared And Global Positioning Systems. http://www.fcc.gov/document/spokesperson-statement-ntia-letter-lightsquared-and-gps. Accessed 14 September 2012

Fortuny-Guasch J, Wildemeersch M, Borio D (2011) Assessment of DVB-T Impact on GNSS Acquisition and Tracking Performance, Proc. ION GNSS ITM, pages 347-356, San Diego, CA

Javad GNSS Inc (2011) A technical story... of a bad filter... and a good filter... which turned political!, Tech.rep., http://javad.com/downloads/javadgnss/publications/20112312.pdf. Accessed 29 September 2012

Kaplan ED, Hegarty CJ (2005) Understanding GPS: Principles and Applications, 2nd edn. Artech House Publishers

NPEF (2012) Follow-on Assessment of LightSquared Ancillary Terrestrial Component Effects on GPS Receivers, Tech. rep., National Space-Based Positioning, Navigation, and Timing Systems Engineering Forum, http://www.gps.gov/news/2012/02/lightsquared/NPEF-report.pdf. Accessed 29 September 2012

NTIA (2012) Letter to the Chairman of the FCC, http://www.ntia.doc.gov/files/ntia/publications/lightsquared_letter_to_chairman_genachowski_-_feb_14_2012.pdf.

Accessed 14 September 2012

Parkinson BW, Spilker JJ (1996) Global Positioning System: Theory and Applications Volume 1, volume 163 of Progress in Astronautics and Aeronautics, American Institute of Astronautics and Aeronautics

Rebeyrol E, Julien O, Macabiau C, Ries L, Delatour A, Lestarquit L (2007) Galileo civil signal modulations, GPS Solutions, 11:159-171

Turetzky G, Rich L, Harris E, Butler K (2012) November 2011 Cellular Device Test Report (with January 26, 2012 Addendum), Tech. rep., NTIA, http://ntl.bts.gov/lib/44000/44300/44300/04_NTIA_Letter_Enclosure_2_-_2012_Jan_26_-_Cellular_Report_to_NTIAOnNov2011_LabTestsOfSelectCellDevices_-_NTIA.pdf. Accessed 14 September 2012

TWG (2011) Lightsquared/GPS Technical Working Group Final Report, Tech. rep., http://apps.fcc.gov/ecfs/document/view?id=7021690471. Accessed 01 October 2012

Biography

Marco Rao is a post-doctoral fellow at the European Commission Joint Research Centre. He obtained his Ph.D. from Università di Palermo and was senoir research associate at the Politecnico di Torino till October 2011. His research interests lie in the area of GNSS signal processing.

Cillian O'Driscoll is a post-doctoral researcher at the Institute for the Protection and Security of the Citizen (IPSC) at the Joint Research Centre (JRC) of the European Commission. His research interests are in all areas of GNSS signal processing.

Daniele Borio received the M.S. and the Ph.D. degree from Politecnico di Torino in 2004 and 2008, respectively. From January 2008 to September 2010 he was a senior research associate in the PLAN group of the University of Calgary, Canada. He is currently a post-doctoral fellow at the Joint Research Centre of the European Commission in the fields of digital and wireless communications, location and navigation.

Joaquim Fortuny (SM IEEE) received the M.S. and the PhD respectively from the Technical University of Catalonia (UPC) and the Universität Karlsruhe (TH). Since 1993, he has been with the European Commission Joint Research Centre, Ispra, Italy, where he is a senior scientific officer. His current research interests are in the fields of testing of GNSS receivers' immunity, spectrum monitoring and geolocation of interference sources.